Mechanism and Machine Theory 58 (2012) 101–119

Contents lists available at SciVerse ScienceDirect

Mechanism and Machine Theory

journal homepage: www.elsevier.com/locate/mechmt

A spring-mass-lever model, stiffness and inertia maps for single-input, single-output compliant mechanisms

Sudarshan Hegde *, G.K. Ananthasuresh

Dept. of Mechanical Engineering, Indian Institute of Science, Bangalore, India

ARTICLE INFO

Article history:
Received 13 December 2010
received in revised form 1 January 2012
accepted 3 January 2012
Available online 7 September 2012

Keywords:
Compliant mechanisms
Spring-leverage model
Selection map

ABSTRACT

A spring-mass-lever (SML) model is introduced in this paper for a single-input-single-output compliant mechanism to capture its static and dynamic behavior. The SML model is a reduced-order model, and its five parameters provide physical insight and quantify the stiffness and inertia[1] at the input and output ports as well as the transformation of force and displacement between the input and output. The model parameters can be determined with reasonable accuracy without performing dynamic or modal analysis. The paper describes two uses of the SML model: computationally efficient analysis of a system of which the compliant mechanism is a part; and design of compliant mechanisms for the given user-specifications. During design, the SML model enables determining the feasible parameter space of user-specified requirements, assessing the suitability of a compliant mechanism to meet the user-specifications and also selecting and/or re-designing compliant mechanisms from an existing database. Manufacturing constraints, material choice, and other practical considerations are incorporated into this methodology. A micromachined accelerometer and a valve mechanism are used as examples to show the effectiveness of the SML model in analysis and design.

© 2012 Published by Elsevier Ltd.

1. Introduction

This paper presents a physically meaningful lumped model for describing the static and dynamic behavior of single-input-single-output compliant mechanisms. Lumped modeling of a continuum or a large system is important in quick design and system-level analysis. It is a common practice in many fields of engineering and science. Electrical and electronics, in particular, have well-established lumped models for continua as well as large systems in terms of their input and output terminal characteristics. A capacitor, a resistor, and an inductor are examples of lumped models defined between two points in a continuum. An operational amplifier, a device with many individual components, has a lumped model with five terminals. In elastic mechanics, vibrations in particular, it is common to represent an elastic continuum as a spring-mass lumped model.

Compliant mechanisms (see Fig. 1; [1]), even in their simplest and most widely used configurations, have two points of interest in addition to the anchored portion(s); input acts as one point (which is called the *input port*) and output is taken at another point (which is called the *output port*). A compliant mechanism transforms the input force and motion and delivers at the output port. Furthermore, it has different stiffness and inertia at its input and output ports. In this paper, we propose a two degree-of-freedom (2-dof) *spring-mass-lever* (SML) model for the elastic continuum of a two-port compliant mechanism to capture its static and dynamic behavior.

* Corresponding author. Tel.: +91 80 22933363.
E-mail addresses: hegde@mecheng.iisc.ernet.in (S. Hegde), suresh@mecheng.iisc.ernet.in (G.K. Ananthasuresh).

[1] This is an extended version of our conference paper at the IFToMM 2011 World Congress, to be held at Mexico.

0094-114X/$ – see front matter © 2012 Published by Elsevier Ltd.
doi:10.1016/j.mechmachtheory.2012.01.006

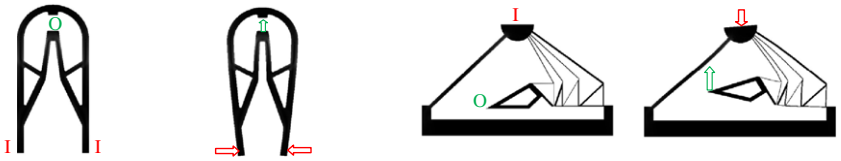

Fig. 1. Compliant mechanisms in original and deformed configurations with input (I) and output (O) ports marked.

The motivation for the SML model arises in two contexts. The first is the computationally efficient analysis of a large system of which the compliant mechanism is a small part. The second is how the quick analysis of a large system helps in the design of a compliant mechanism as per user-specifications of a given application. In this paper, we explain both aspects with the help of two applications where a compliant mechanism is used.

1.1. Motivating example 1

Consider a capacitive micromachined accelerometer as shown in Fig. 2. It consists of a large mass, a *proof-mass*, attached to a flexible suspension, and also to a moving set of electrostatic combs, which has its own suspension through a *displacement-amplifying compliant mechanism* (DaCM). The input acceleration causes the proof mass and the suspensions to deform. The relative motion between the stationary set of combs and the moving set of combs results in change in capacitance, which is read by the electronic circuitry. The DaCM amplifies the displacement of the proof-mass. Since the capacitance measured is a function of the displacement of the moving set of combs, the sensitivity of the accelerometer could be improved by adding a DaCM between the proof-mass and the comb-drive. Sensing electrical capacitance at the output of the DaCM gives rise to a more sensitive accelerometer than the one in which capacitance is measured directly at the proof-mass.

In order to estimate the performance parameters of the accelerometer such as sensitivity, resolution, time-constant, bandwidth, etc., the static and dynamic behavior of this accelerometer needs to be simulated. Using finite element analysis (FEA) of the complete device will be computationally expensive, especially when this accelerometer is to be co-simulated along with its electronics. A lumped model is useful in such situations. Modeling of the stiffness and inertia of single-port elastic structures (the suspensions of the mass and the sensing side), shown in Fig. 2, is straightforward and is well understood. Presenting such a model that captures the two-port elastic structure such as the DaCM is the focus of this work. It is shown schematically as a lever in Fig. 2 to signify the amplification. But it is a constrained lever with stiffness and inertia at its input and output sides. This provides a pointer to a spring-mass-lever (SML) model.

1.2. Motivating Example 2

Consider an actuator which can produce a constant force in the form of a step excitation of magnitude 1 N over a displacement of 0.001 m. Fig. 3 shows the valve mechanism actuated by this actuator. The displacement of the actuator can be amplified by a DaCM attached to it. The design of a DaCM that amplifies the displacement of the actuator to give the prescribed displacement at the output against a prescribed output load is the goal here. The output is required to move by a distance of 0.01 m when the input moves by 0.001 m, an amplification of 10 times, against a steady load of 0.02 N at the output. This is possible energetically because the input energy is 1×10^{-3} J while the work done at the output is 2×10^{-4} J. The remaining energy goes in the

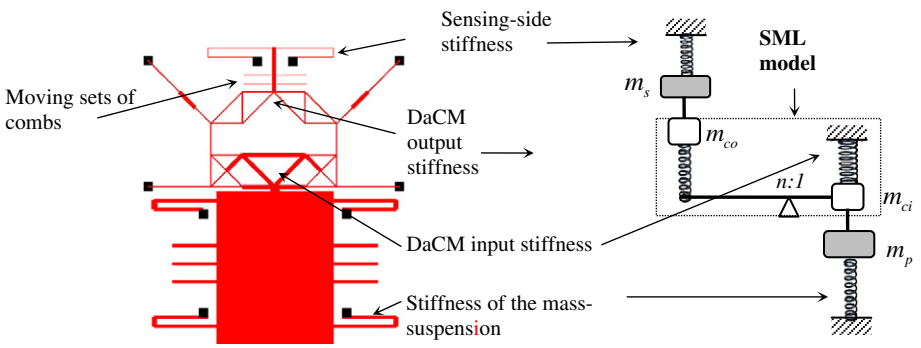

Fig. 2. Schematic of a micromachined accelerometer and its lumped model; the subscripts p and s represent proof-mass and suspension respectively.

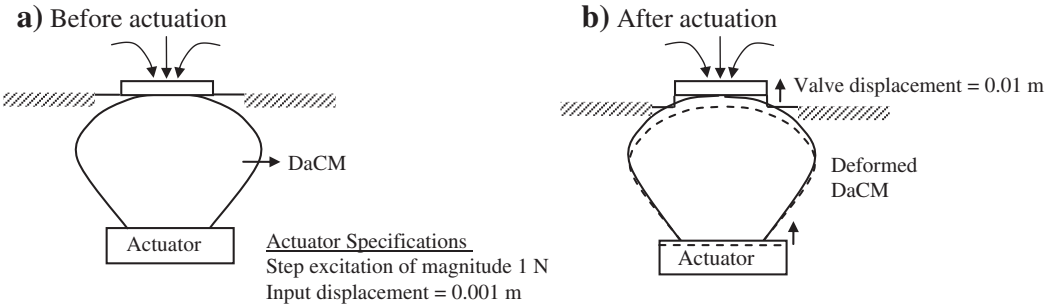

Fig. 3. Pictorial depiction of a miniature valve with an actuator.

deformation of the compliant mechanism. But is this transformation from input to output possible within the prescribed space and prescribed switching time? This and a few more questions arise in the context of this example and the example 1.

1. Can the specifications be met by a compliant mechanism?
2. Can any existing compliant mechanism designs meet these specifications? If not, how far are they from meeting these specifications?
3. How can one design a compliant mechanism that meets the specifications, identify material and manufacturing process for it, and also satisfy other performance and practical requirements?

Existing methods for compliant mechanism design (see subsection 1.1) are oriented towards addressing the third question rather than the first two questions. By introducing the concepts of stiffness and inertia maps that depict the feasibility of user-specifications of the kind mentioned in the aforementioned motivating example problems, we answer not only the first two questions but also address the third.

In order to contrast the analysis and design methods using the SML model presented in the paper, it is pertinent to provide a brief overview of the existing methods.

1.3. Related work

Analysis and design of compliant mechanisms require due attention to kinematics and kinetics of elastic deformations [1]. Different methods have emerged in the last two decades. One, known as the *pseudo-rigid-body model* approach [1–3], models elastic effects using a lumped torsional spring at a revolute joint and uses the well-established principles of kinematic analysis and design with appropriate changes as necessary. It has been applied to a number of practical applications [1] and is also extended beyond planar applications to spatial [4] and spherical [5] linkages. Another approach is to use continuum elastic mechanics directly where kinematics is inherently accounted for. Finite element analysis is used for the simulations in this approach. Systematic design methods based on this approach [6,7] and their many extensions use optimization, topology optimization [8,9] in particular. In spite of the computational complexity, this method has been applied to practical applications (e.g., [10,11]). Newer approaches are now emerging wherein building blocks are used to develop compliant designs [12].

All of the aforementioned methods aim to develop a compliant design anew whenever a new problem is posed. Occasionally, an existing compliant design may be used as a starting point for a new design. As noted earlier, it is fair to say that all these methods are not capable of informing a designer a priori whether a particular set of specifications can be met or not; one has to try and see if the design method converges to an acceptable solution.

In contrast, the approach presented in this paper aims to show the feasibility of specifications in terms of the SML model parameters and also helps design a new compliant mechanism using selection among a known set of existing designs stored in a database, most of which are designed using the aforementioned methods. The method also re-designs the selected mechanism in an interactive graphics-based framework to satisfy the user-specifications. The SML model and the design methodology presented in this paper are extensions of our authors' recent work reported in [11,13].

1.4. Organization of the paper

The SML model is presented in Section 2. The use of SML model in the device-level analysis is illustrated in Section 3. This is done with the help of two examples; a micromachined accelerometer and a compliant transient valve. The same examples are then used in Section 4 to present the use of SML model in the design of complaint mechanisms. It also introduces the stiffness and inertia maps. Closure is given in Section 5.

2. Spring-mass-lever (SML) model

The spring-lever model (SL) proposed in [11,13] is for static analysis. It had the input-side spring stiffness k_{ci}, the output-side spring stiffness k_{co}, and a lever with an amplification factor n. These three parameters are similar to the three stiffness parameters

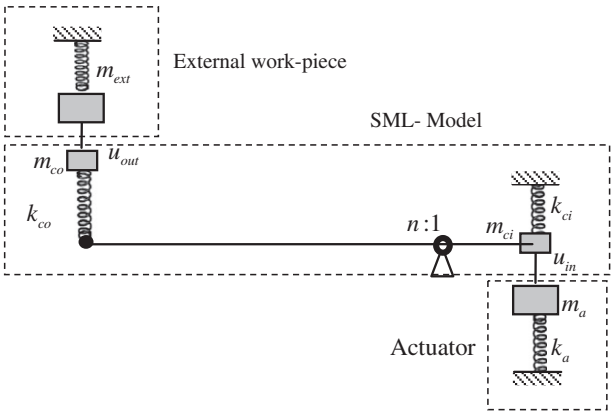

Fig. 4. An SML model; apart from the input side and output side stiffnesses and lever ratio, the SML model consists of inertia terms $m_{ci}$and m_{co}.

that exist in the symmetric 2×2 stiffness matrix that relate the input–output forces and their respective displacements (for example, see [14]). The stiffness inherent in the actuator was modeled in [11] as k_a and that of the output due to a work-piece as k_{ext}.

In an SML model, input and output inertias are added as lumped masses, one at the input port as m_{ci}, and the other at the output port as m_{co}. The inertia arising from the actuation side is included as m_a and that due to the output as m_{ext}. The SML model is shown in Fig. 4.

The four parameters (k_a, m_a, k_{ext}, and m_{ext}) pertain to single-port elements (i.e., actuator and the work-piece) and are easily amenable to standard spring-mass model shown in Fig. 1. On the other hand, we need five parameters (i.e., k_{ci}, m_{ci},k_{co}, m_{co}, and n) to capture the functional intent of a compliant mechanism. These parameters need to be determined to correctly capture the strain and kinematic energies of the entire compliant mechanism in terms of its lumped degrees of freedom at the input and output ports. The last parameter, n, accounts for the transformation that happens between the input and the output.

An SML model shown in Fig. 4 has two degrees of freedom (dofs). Let there be an input force F_{in} and an output force F_{out} at the input and output ports respectively. And, let the corresponding displacements be u_{in} and u_{out}. By applying static equilibrium condition to this two-dof SML model of Fig. 4, we obtain [13]:

$$k_{ci} = \frac{F_{in} - k_a u_{in} - n(k_{ext} u_{out} - F_{out})}{u_{in}} \tag{1}$$

$$k_{co} = \frac{(k_{ext} u_{out} - F_{out})}{n u_{in} - u_{out}} \tag{2}$$

The preceding equations are helpful in finding the stiffness parameters of the SML model. For this we need to perform two static FEA runs of the complete meshed model of a compliant mechanism without the actuator and workpiece. The first FEA run has only F_{in} applied at the input dof. With this, we obtain displacements at its input and output displacements. The ratio of the output displacement to that at the input leads to the inherent amplification, n. This is the lever ratio shown in Fig. 4. Once we know n, k_{ci} is computed using Eq. (1). Note that, k_a, k_{ext}, and F_{out} are all zero for this step. Hence, $k_{ci} = F_{in}/u_{in}$.

In the second FEA run, we apply only F_{out} by keeping $F_{in} = 0$. Once again, k_a and k_{ext} are zero because the actuator and the work-piece are excluded in this FEA run too because we want to capture only the behavior of the compliant mechanism. We get u_{in} and u_{out} in this FEA run. We substitute them in Eq. (2) to get k_{co}. It was shown in [11,13] that k_{ci} and k_{co} determined in this manner result in equal strain energies in the FEA model of the full compliant mechanism and the SML model. Now, to determine m_{ci} and m_{co}, we have two options as described next.

In the first method, we can perform modal analysis of the FEA meshed model and equate the first two natural frequencies to the two natural frequencies obtained with the SML model. Referring to Fig. 4, the SML equations are derived by first writing the Lagrangian for the system and then applying the Euler-Lagrange (E-L) equations to it to get

$$\begin{pmatrix} m_{ci}+m_a & 0 \\ 0 & m_{co}+m_{ext} \end{pmatrix} \begin{pmatrix} \ddot{u}_{in} \\ \ddot{u}_{out} \end{pmatrix} + \begin{pmatrix} k_{ci}+k_a+n^2 k_{co} & -nk_{co} \\ -nk_{co} & k_{ext}+k_{co} \end{pmatrix} \begin{pmatrix} u_{in} \\ u_{out} \end{pmatrix} = 0 \tag{3}$$

The expressions for the natural frequencies can be obtained from the set of equations in Eq. (3) and are obtained as follows:

$$\omega_1{}^2 = \left(\frac{k_{ci}+k_a+n^2k_{co}}{2(m_{ci}+m_a)}+\frac{k_{ext}+k_{co}}{2(m_{co}+m_{ext})}\right)-\sqrt{\left(\frac{k_{ci}+k_a+n^2k_{co}}{2(m_{ci}+m_a)}-\frac{k_{ext}+k_{co}}{2(m_{co}+m_{ext})}\right)^2+\frac{(nk_{co})^2}{(m_{co}+m_{ext})(m_{ci}+m_a)}} \tag{4a}$$

and

$$\omega_2{}^2 = \left(\frac{k_{ci}+k_a+n^2k_{co}}{2(m_{ci}+m_a)}+\frac{k_{ext}+k_{co}}{2(m_{co}+m_{ext})}\right)+\sqrt{\left(\frac{k_{ci}+k_a+n^2k_{co}}{2(m_{ci}+m_a)}-\frac{k_{ext}+k_{co}}{2(m_{co}+m_{ext})}\right)^2+\frac{(nk_{co})^2}{(m_{co}+m_{ext})(m_{ci}+m_a)}} \tag{4b}$$

Eq. (3) can be also be used to derive the ratio of the modal displacements at the output and input, and is given by

$$\frac{\hat{u}_{out}}{\hat{u}_{in}} = \frac{nk_{co}}{k_{ext}+k_{co}-(m_{co}+m_{ext})\omega^2} \tag{5}$$

Once again, we take $k_a = m_a = k_{ext} = m_{ext} = 0$ since the actuator and the work-piece are excluded. And, we take k_{ci}, k_{co} and n of the SML model as determined from two static FEA runs. With these, Eqs. (4a) and (4b) lead to two equations in terms of m_{ci} and m_{co} when we substitute for ω_1 and ω_2 as numerical values of the first two natural frequencies as determined by the modal analysis run of the FEA model.

But modal analysis is computationally expensive. It should be avoided because extraction of m_{ci} and m_{co} needs to be done quickly in re-designing a compliant mechanism as described later. Hence, an approximation is used in the second method of estimating m_{ci} and m_{co}. Here, we perform only two static FEA runs — the same two that are to be done for determining k_{ci} and k_{co}. We consider displacements of all degrees of freedom of the FEA model in both runs. Let them be denoted by vectors $\mathbf{U}_1$ and $\mathbf{U}_2$, respectively. We now equate the kinetic energies of the SML model and those of the full FEA model.

$$\frac{1}{2}m_{ci}u_{in1}{}^2+\frac{1}{2}m_{co}u_{out1}{}^2=\frac{\rho}{2}\sum_{i=1}^{N}U_{1i}^2v_i \tag{6a}$$

$$\frac{1}{2}m_{ci}u_{in2}{}^2+\frac{1}{2}m_{co}u_{out2}{}^2=\frac{\rho}{2}\sum_{i=1}^{N}U_{2i}^2v_i \tag{6b}$$

where v_i is the volume associated with the ith finite element, ρ is the density of material of the compliant mechanism, and subscripts 1 and 2 refer to the static FEA runs 1 and 2. Eq. (6a)–(6b) are solved to determine m_{ci} and m_{co}. When we substitute these and known values of the other parameters into Eqs. (4a) and (4b), we obtain the natural frequencies of the SML model. These will not be exactly the same as the first two natural frequencies as determined by the full FEA modal analysis but they will be sufficiently close. The closeness or discrepancy is related to how similar first two normal modes of the full FEA model are to the static deformation modes of the two static FEA runs.

By noting that the natural frequency is not significantly influenced by the normal mode shape, we contend that the error in estimated frequencies of the SML model using m_{ci} and m_{co} determined using the second method are accurate enough. Numerical experiments with different compliant mechanisms confirmed this fact wherein the discrepancy between the first two natural frequencies of the full FEA model agreed with the two natural frequencies of the SML model within 2%. We show two specific examples to validate the method of finding the inertia parameters m_{ci} and m_{co} of the SML model in Section 3. More interestingly, as shown in Section 3, the transient response of the SML model is in reasonable agreement with that of the input and output dofs of the full FEA model, as described later.

3. SML model in analysis

In this section, we use the example of a capacitive micromachined accelerometer and a compliant valve to illustrate the use of the SML model in the analysis of a device.

3.1. Analysis of micromachined accelerometer

The use of an SML model in the quick analysis of a large device is illustrated with the help of two designs of accelerometers, S_1 and S_2, having DaCMs M_1 and M_2 respectively, as shown in Fig. 5. The following three quantities are computed using the SML model and the complete FEA model and compared: (i) frequency of the overall system, (ii) frequency of the DaCM alone, and (iii) the ratio of the modal displacements at the output and input. The results are tabulated in Table 1. Results show that the three aforementioned performance parameters that are calculated using the expressions for the SML model match closely with the complete FE model with a maximum error of about 2%.

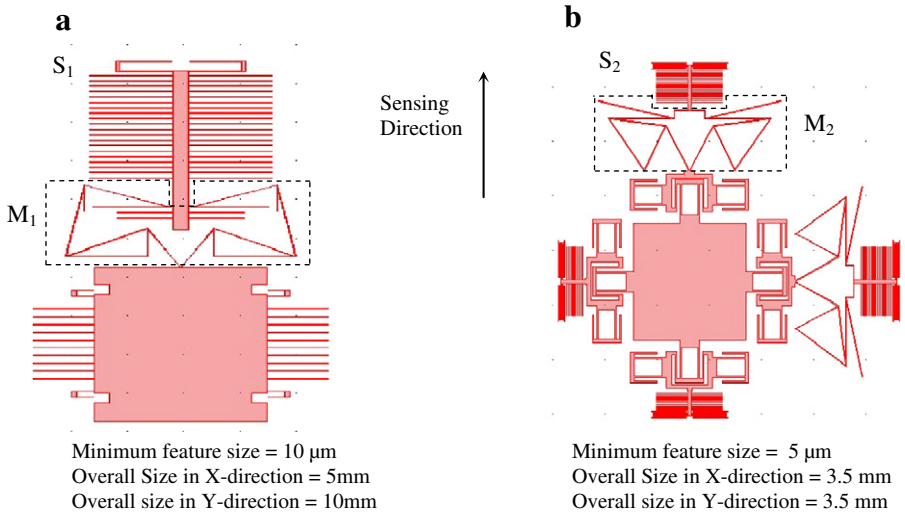

Fig. 5. The two accelerometer designs S_1 and S_2 with DaCMs M_1 and M_2 respectively.

In the case of an accelerometer, the proof-mass plays the role of an actuator, and the sensing-side suspension plays the role of a work-piece. In these computations, the stiffness and inertia of the input-side (k_a and m_a) and sensing-side (k_{ext} and m_{ext}) suspensions are modeled as single-port elastic structures. Their values are given in Appendix A (Tables A1 and A2). Using these values and the SML parameters given in Table A3 of Appendix A, the frequency of the overall device is calculated using Eq. (4a). The frequency of the DaCM alone is calculated from Eq. (4a) by using the substitution $k_a = m_a = k_{ext} = m_{ext} = 0$. The ratio of modal displacements is calculated using Eq. (5).

Table 1
Comparison of frequencies for accelerometer designs S1 and S2, with DaCMs M1 and M2 respectively of Fig. 5(a) and (b).

Attribute	Complete FE model	SML model	% error
u_{out}/u_{in} of entire system S_1 with mechanism M_1	56.03	56.08	−0.09
ω of entire system S_1 with mechanism M_1 (Hz)	482.22	472.05	2.1
ω of DaCM M_1 alone (Hz)	4069.49	4130.6	−1.5
u_{out}/u_{in} of entire system S_2 with mechanism M_2	−7.09	−7.25	−2.25
ω of entire system S_2 with Mechanism M_2 (Hz)	23061.15	22846.53	0.93
ω of DaCM M_2 alone (Hz)	5360.83	5266.99	1.75

Table A1
Input side calculations.

Device	Eigenfrequency (Hz)	Stiffness k_a (N/m)	Effective mass m_a (kg)
S_1	918.10	77.53	2.33×10^{-6}
S_2	35159	3806.33	7.80×10^{-8}

Table A2
Output side calculations.

Device	Eigenfrequency (Hz)	Stiffness k_{ext} (N/m)	Effective mass m_{ext} (kg)
S_1	331.24	0.58	1.34×10^{-7}
S_2	10990.84	17.67	3.70×10^{-9}

Table A3
Calculation of m_{ci} and m_{co}.

Mechanism	TKE (1st loading case)	TKE (2nd loading case)	m_{ci} (kg)	m_{co} (kg)
M_1	4.09×10^{-13}	1.27×10^{-9}	7.84×10^{-8}	8.43×10^{-10}
M_2	1.57×10^{-14}	5.98×10^{-13}	4.22×10^{-9}	2.40×10^{-10}

The static equilibrium equations (Eqs. (1)–(2)) of the SML model also provide useful insights into the behavior of the device. For example, how the stiffness of the sensing-side suspension affects the output side displacement? Consider a case where the DaCM with the lumped parameters, $k_{ci}=4.75\times10^{2}$ N/m, $k_{co}=1.85\times10^{2}$ N/m and $n=5.56$, is used with $m_a=1\times10^{-7}$ kg, $m_{ext}=6\times10^{-8}$ kg and $k_a=200$ N/m. In this case, the input force and output force are taken as $m_a a$ and $m_{ext}a$ respectively, and the output displacement for a given acceleration a is given by

$$u_{out}=\frac{\left(k_{co}nm_a\pm m_{ext}k_{ci}\pm m_{ext}k_a\pm m_{ext}n^2k_{co}\right)a}{\left(k_{co}k_{ci}+k_{co}k_a+k_{ext}k_{ci}+k_{ext}k_a+n^2k_{ext}k_{co}\right)} \tag{7}$$

where the negative sign refers to the case of an inverting mechanism.

Fig. 6 shows a plot of two quantities: i) the ratio of output side displacement to the applied acceleration and ii) the external suspension stiffness. This gives a quantitative idea as to how the external stiffness affects the output displacement. This also confirms that a non-inverting mechanism fares better than an inverting mechanism, where the inertia load is applied in the opposite direction of the measured output displacement.

Consider a situation, as shown in Fig. 7, where the input suspension (k_a and m_a) and the sensing-side suspension (k_{ext} and m_{ext}) are chosen by the designer. Different DaCMs in the database, as shown in Fig. 7, with their pre-computed SL parameters, can be potentially used. The output displacements obtained with different DaCMs can be found easily by using Eq. (7) and are listed in Fig. 7, with mechanism 2 being the best and 3 being the worst. This provides a pointer to the use of the SML model in the design of accelerometer based on selection of DaCMs from a database.

3.2. Transient analysis of compliant valve

In some applications, there is a requirement that the input and output ports reach certain displacement values within a given time t. To address such situations, the transient response of the compliant mechanism predicted by the SML model, under a time-varying force is illustrated in this section. Similar to free vibration equations i.e. Eq. (3), the equilibrium equations for the SML model under an application of a time-dependent force, $F_{in}(t)$ and $F_{out}(t)$at the input and output ports respectively, in the matrix form are:

$$\begin{pmatrix} m_{ci}+m_a & 0 \\ 0 & m_{co}+m_{ext}\end{pmatrix}\begin{Bmatrix}\ddot{u}_{in}\\ \ddot{u}_{out}\end{Bmatrix}+\begin{pmatrix} k_{ci}+n^2k_{co}+k_a & -nk_{co} \\ -nk_{co} & k_{co}+k_{ext}\end{pmatrix}\begin{Bmatrix}u_{in}\\ u_{out}\end{Bmatrix}=\begin{Bmatrix}F_{in}\\ F_{out}\end{Bmatrix} \tag{8}$$

Here, the structural damping is assumed to be zero. In order to solve for $u_{in}(t)$ and $u_{out}(t)$, the two coupled equations (Eq. (8)) can be decoupled using a substitution

$$\mathbf{u}=\mathbf{Pq} \tag{9}$$

where $\mathbf{P}$ is the normal mode matrix. The first and second columns of the 2×2 matrix $\mathbf{P}$ contain the eigenvectors of the matrix systems in Eq. (8) with the right-hand-side zero. The decoupled equations are solved for the modal coordinates $\mathbf{q}$. The decoupled equations are given by

$$\begin{bmatrix} m_{11} & 0 \\ 0 & m_{22}\end{bmatrix}\begin{Bmatrix}\ddot{q}_1\\ \ddot{q}_2\end{Bmatrix}+\begin{bmatrix} K_{11} & 0 \\ 0 & K_{22}\end{bmatrix}\begin{Bmatrix}q_1\\ q_2\end{Bmatrix}=\begin{Bmatrix}f_1\\ f_2\end{Bmatrix} \tag{10}$$

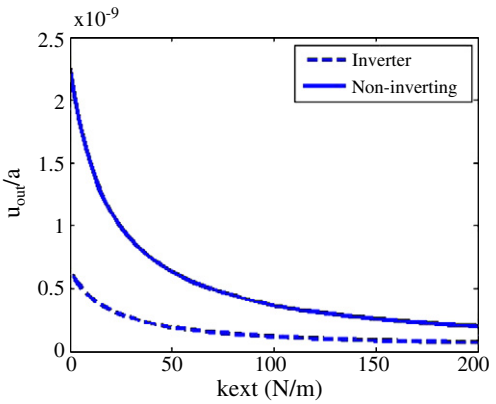

Fig. 6. The u_{out}/a vs suspension-side stiffness (k_{ext}) in the case of a inverting and non-inverting mechanism.

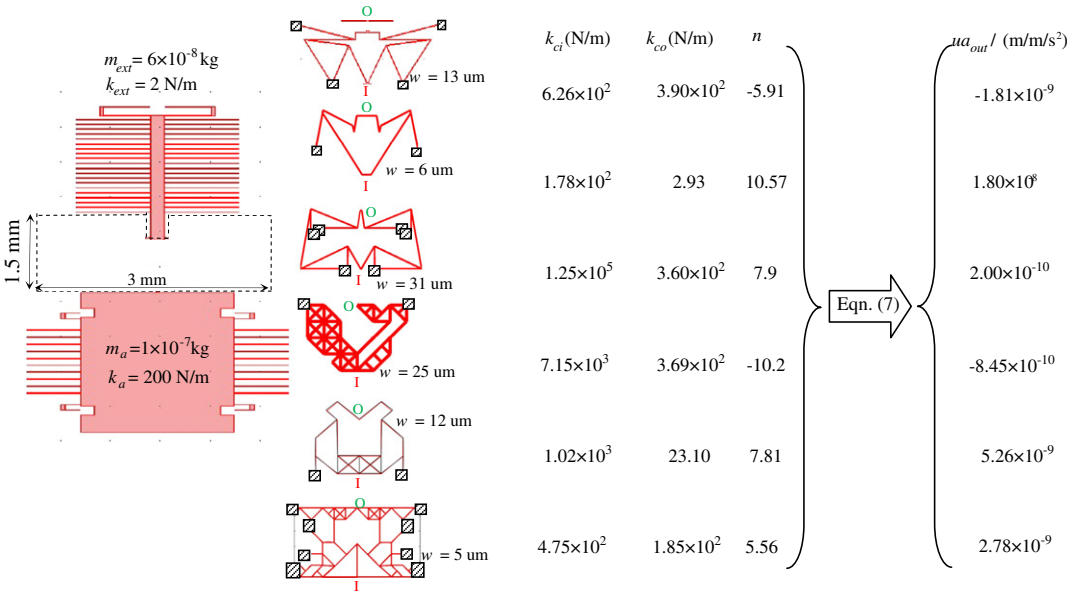

Fig. 7. A single equation can be used to compute the output displacement from the pre-computed values of the SL parameters of the DaCMs.

where the expressions for the terms and symbols that appear in the above equations (and subsequent equations, Eqs. (11)–(13)) are tabulated in Appendix B. When the forcing function is in the form of a step excitation, the solution for **q** in Eq. (10) is given by

$$q_i = \frac{f_i}{K_{ii}}\left(1-\cos\left(\sqrt{\frac{K_{ii}}{m_{ii}}}t\right)\right), i = 1..2 \tag{11}$$

The modal coordinates **q** are then transformed to **u** using the transformation equation (Eq. (9)) to get the response.

A compliant mechanism shown in Fig. 8 is considered for analysis here. Its SML parameters are as follows: k_{ci} = 1054.2 N/m, k_{co} = 24.6 N/m, m_{ci} = 0.074 kg, m_{co} = 0.0031 kg and n = 7.4. The forcing function is a step excitation of magnitude 20 N applied at the input port. The displacements at the input and the output ports as a function of time, obtained using the FEA and the SML model-based analyses, are shown in Fig. 9. As can be seen in the plots of Fig. 9, we get reasonable match of the responses between those predicted by the SML model and the complete FE model: the maximum mismatch relative to the maximum displacement for the input displacement was 18% and that at the output was 2%. The difference in the response behavior is due to the difference in the static deformation profile and the mode shape, as mentioned earlier.

Eq. (11) can be used to solve for the time taken t and is given as

$$t = \frac{\pi - \cos^{-1}\left(\frac{K_{11}q_1 - f_1}{f_1}\right)}{\sqrt{\frac{K_{11}}{m_{11}}}} \tag{12}$$

The above equation is in terms of modal coordinates **q**. The modal coordinates **q** is then transformed to **u**. The time taken by the input and the output port to reach a certain specified displacements u_{in} and u_{out} respectively is given by

$$t = \frac{\pi - \cos^{-1}\left(\frac{K_{11}(\phi_{11}u_{in} + \phi_{12}u_{out}) - f_1}{f_1}\right)}{\sqrt{\frac{K_{11}}{m_{11}}}} \tag{13}$$

Thus, we can use a single equation, i.e., Eq. (13) which is in terms of the five SML constants and other specification variables to calculate the time taken by the input and output ports of the compliant mechanism to undergo given displacements.

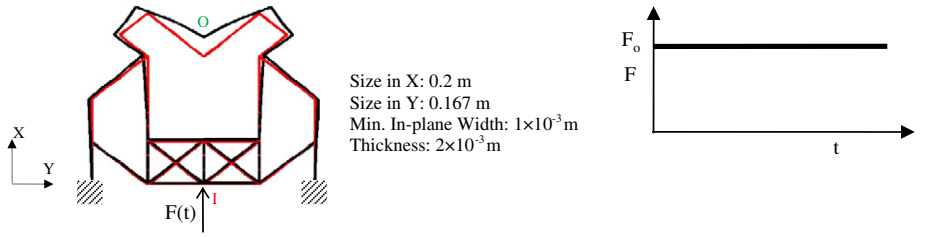

Fig. 8. The compliant mechanism considered for the transient response under a step forcing function at the input port.

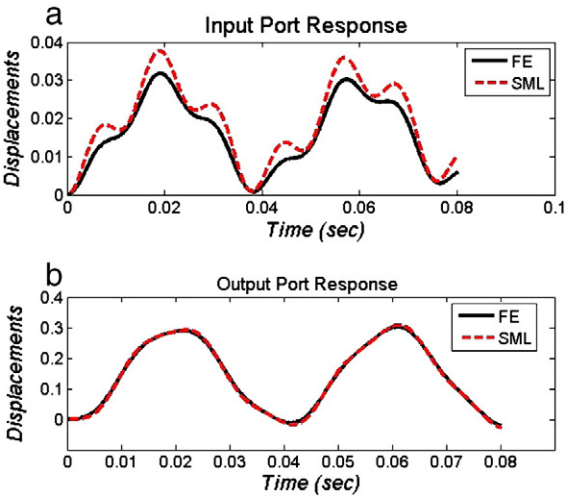

Fig. 9. The response behavior at (a) the input port and (b) the output port predicted by the SML model and the complete FE model.

4. Use of the SML model in design

In this section, we use the example of a micromachined accelerometer and miniature compliant valve mechanism illustrated in Section 1 to show the use of SML model in the quick design of compliant mechanisms. We also illustrate the use of SML model in assessing the feasibility of user-specifications for a compliant mechanism. Stiffness and inertia maps are introduced in the context of design.

4.1. Selection and re-design methodology

The methodology adopted is an extension of our recent work [13] to consider dynamic behavior. It consists of two steps: (i) computing the feasible sets of the five SML parameters that satisfy user-specifications, and (ii) selecting and/or re-designing a compliant mechanism such that its SML parameters fall within the feasible set as determined in the first step. Our earlier work [13] involved computing the feasible set of only three parameters and selecting and/or re-designing the mechanism such that its three parameters match with the feasible set of three parameters.

The method starts with the problem specifications entered by the user as shown in Fig. 10. These user-specifications relate to the desired functionality of the compliant mechanism. They include, as can be seen in the left-most box in Fig. 10, the input force (F_{in}), input displacement (u_{in}), output load (F_{out}), and output displacement (u_{out}). Depending on the problem, additional user-specifications such as actuator stiffness (k_a), external stiffness (k_{ext}), actuator inertia (m_a), external inertia (m_{ext}), natural frequency (ω), response time to reach a desired state (t), etc., may also be relevant. In a design problem, the user may want to exercise some freedom in specifying the numerical values for some of these quantities. Therefore, the user is given the option of specifying a range for each quantity as indicated in Fig. 10.

The next step is to write the equations that govern the desired function. Equality expressions that govern the desired functionality would involve the user-specification variables as well as the SML parameters.

$$h_i(\mathbf{s}, k_{ci}, k_{co}, m_{ci}, m_{co}, n) = 0, \quad i = 1, 2, \cdots, n_{eq} \tag{14}$$

where $\mathbf{s}$ is $n_s \times 1$ array of n_s user-specifications, $h_{i=1\cdots n_{eq}}$ the governing equations, n_{eq} the number of equations. Eq. (14) will be over-constrained if $n_{eq} > n_s$ and there will not be a solution in general. If $n_{eq} \leq n_s$, many solutions may exist. Additionally, as noted earlier and can be seen in Fig. 10, each variable in $\mathbf{s}$ has upper and lower bounds, which leads to $2n_s$ more inequalities.

$$s_i^{\min} \leq s_i \leq s_i^{\max}, \quad i = 1, 2, \cdots, n_s \tag{15}$$

Therefore, Eqs. (14)–(15) are to be solved to find the feasible sets of the SML parameters, $\{k_{ci}, k_{co}, m_{ci}, m_{co}, n\}$. Whenever the 5D space of the feasible sets of the SML parameters is not null, it means that the user-specifications are mathematically possible. In reality, we would require further that $\{k_{ci}, k_{co}, m_{ci}, m_{co}\}$ be positive. Note that the inherent amplification factor, n, can be positive or negative resulting in non-inverting and inverting compliant mechanisms. In practice, however, one may impose upper and lower limits on n. Feasible values of the 5D set, $\{k_{ci}, k_{co}, m_{ci}, m_{co}, n\}$, can be graphically visualized in 2D space using *stiffness* and *inertia maps* as described next.

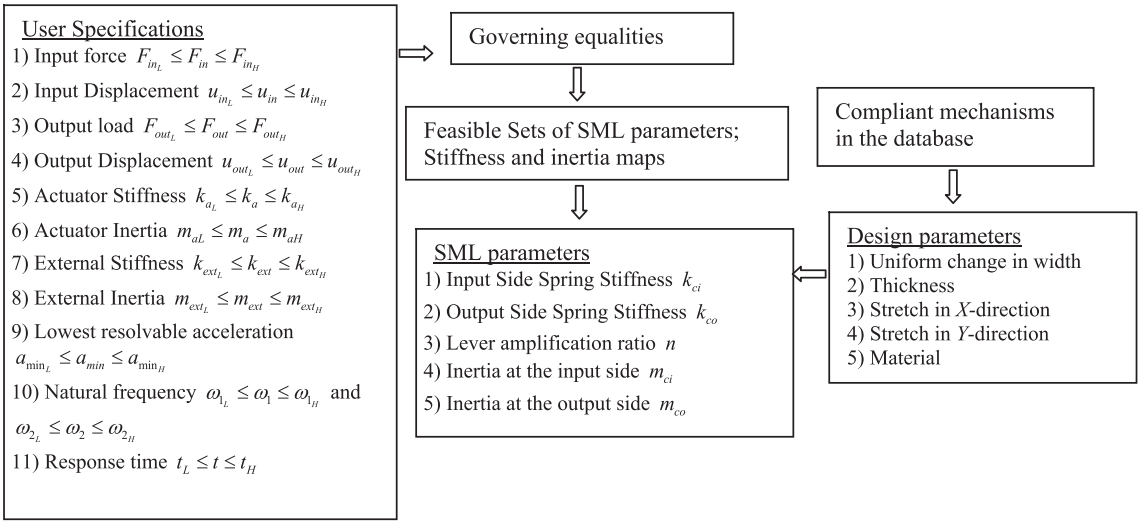

Fig. 10. The user-specifications, SML parameters and the design parameters of the compliant mechanism.

4.1.1. Stiffness and inertia maps

The feasible values of k_{ci}, k_{co} and n are used to create the *stiffness map* on a $k_{ci}-k_{co}$ graph as shown in Fig. 11(a) by solving Eqs. (14)–(15) for all their solutions. The values of $\{m_{ci}, m_{co}\}$, indicated with a cursor ⊕ in the $m_{ci}-m_{co}$ inertia plot, are kept constant in creating this map. If the $\{m_{ci}, m_{co}\}$ corresponds to a mechanism's m_{ci} and m_{co}, the stiffness map suggests the feasible sets of k_{ci}, k_{co} and n for that mechanism, that would satisfy the user-specifications. Note that each point (k_{ci},k_{co}) inside the feasible map may correspond to one or more values of n. In a graphical user interface (GUI) framework, the range of n can be shown when a point is selected inside the feasible space. Similarly, the *inertia map* can be created for the same user-specifications as shown in Fig. 11(b) for some values of $\{k_{ci}, k_{co}\}$. The assumed values of $\{k_{ci}, k_{co}\}$ are indicated with a cursor ⊕ in the stiffness plot. When the cursor ⊕ is moved in the inertia plot, the stiffness map will change; likewise, the inertia map would change when the cursor in the stiffness plot is moved. This helps us to see if any mechanism in the database already satisfies the user-specifications and if this does not happen, to choose the best mechanism that could be further re-designed to meet the specifications. This is explained next.

Recall that each compliant mechanism has a unique set of SML parameters $\{k_{ci}, k_{co}, m_{ci}, m_{co}, n\}$ associated with it. Therefore, each compliant mechanism can be shown as a point in the stiffness and inertia maps. The small circles in Fig. 11(a–b) indicate compliant mechanisms, M_1, …, M_5. In order to see how different mechanisms fare against the user specifications, the cursor ⊕ in the inertia plot is moved from one mechanism to the other, one after the other, and the distance of the mechanism's (k_{ci},k_{co}) from the feasible stiffness map is calculated. The mechanisms are numbered based on these distances. During this process, if any of the mechanism's (k_{ci},k_{co}) lies inside the feasible map with its n value lying between the n values corresponding to the point on the map, the mechanism satisfies the user specifications. Fig. 11(a) shows that mechanism M_1 is feasible in the stiffness plot. If several such mechanisms are found, the user has the freedom to select anyone of them. Practical considerations such as the

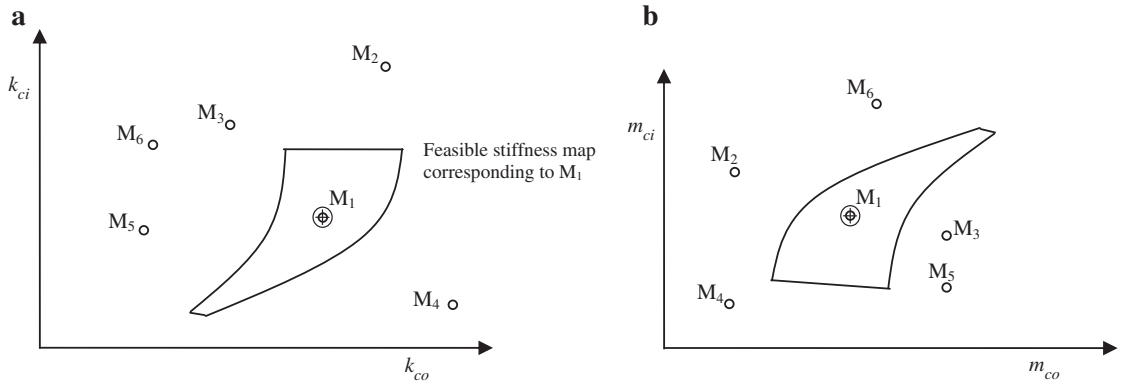

Fig. 11. The feasible stiffness and inertia maps for user-specifications for the design of compliant mechanisms.

overall size, minimum feature size, material, manufacturing process, etc., determine that choice. Performance requirements such as maximum stress are also important. Furthermore, the layout (or topology), the anchored portions, the locations of input and output ports, and the orientations of the input and output dofs also play a role. All of these can be shown to the user in a GUI framework.

If the practical considerations are not obeyed by the candidate designs or none of the mechanisms in the database satisfy the user-specifications readily, the user may opt to re-design (as explained in the next sub-section) them or others that are close to satisfying the functional requirements. In doing so, the mechanism which is closest to its map according to the aforementioned calculated distances is selected for re-design. Once the mechanism is selected for re-design, stiffness map always corresponds to the cursor location in the inertia plot at the mechanism's m_{ci} and m_{co}.

Alternatively, the aforementioned process can be done by measuring the distances of the mechanism's (m_{ci},m_{co}) from the corresponding feasible inertia map. Once the mechanism is selected, the inertia map corresponds to the cursor location in the stiffness plot at the mechanism's (k_{ci},k_{co}).

The re-design of a selected mechanism can take place with the help of either of the two maps. The nature of the equalities governs how easy it is to generate and use one of the two maps. In the case studies that are presented in Subsection 4.2, during the re-design of the mechanism, we work with the feasible stiffness maps only.

This answers the first of the three questions posed in Section 1.2. We will now discuss how to answer the second question: *can any existing compliant mechanisms meet the user-specifications?*

4.1.2. Re-design of a chosen mechanism

When the compliant mechanisms in the database comprise only networks of slender beam-like segments (see Figs. 1, 2, 5 and 7), there exist simple re-design parameters: lengths, widths, and thicknesses. A sample list of re-design parameters are shown in one of the boxes of Fig. 10. They can be interactively changed while observing how the small circles corresponding to the mechanism move in the stiffness and inertia plots. The mechanism's circles move because the SML parameters {k_{ci}, k_{co}, m_{ci}, m_{co}} change when the re-design parameters are varied. This can be visually portrayed in the stiffness and inertia plots with the help of parameter curves shown in Fig. 12(a–b).

By referring to Figs. 11(a) and 12(a), it can be seen that mechanism M_3 is brought into the feasible stiffness map (from M_{31} to M_{32}) by first following parameter curve 1 and then parameter curve 2. The corresponding movement in the inertia plot can also be seen in Fig. 12(b). Since the aforementioned practical and performance considerations are made visible to the user during the re-design process, the selection and re-design methodology yields a practically viable solution. Thus, the third question posed in Section 1.2 is also addressed by this method.

The discussion of the two motivating examples introduced in Sections 1.1 and 1.2 illustrate the specifics of the general methodology described in this section.

4.2. Design of a micromachined accelerometer

The SML and the re-design parameters in the design of a micromachined accelerometer are the same as those given in Fig. 10. The user-specifications for the micromachined accelerometer is a subset of the specifications given in Fig. 10, and are further elaborated here. The user has control over the sensitivity of the accelerometer in specifying the lowest resolvable acceleration $a_{\min}$ and the output displacement u_{out}. This is because the output displacement is sensed by measuring the capacitance. The natural frequency ω_1 is also important because of the bandwidth requirements. At the input side, there is mass of the actuator (i.e., proof-mass that experiences inertial force) m_a with a suspension stiffness k_a, which exerts an input force on the DaCM. At the output side, there is mass and stiffness of the external suspension, m_{ext} and k_{ext}, respectively. Although it may be important to consider the second natural frequency in some applications, we do not consider ω_2 in this discussion.

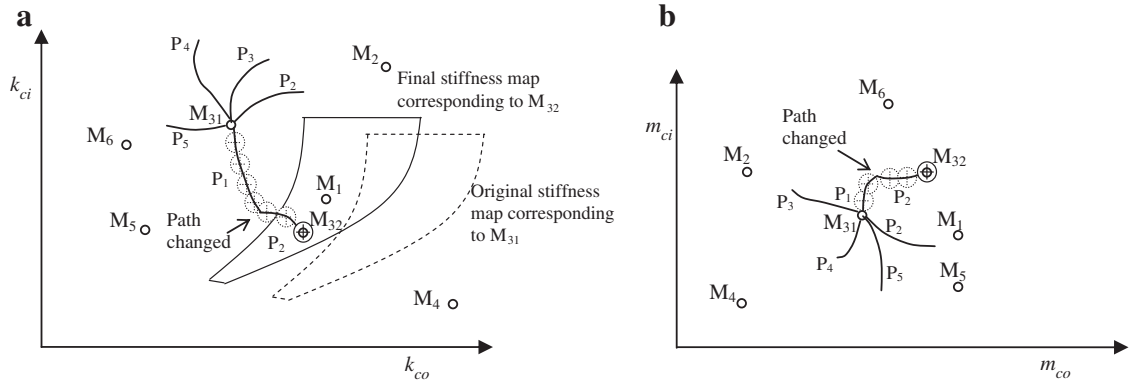

Fig. 12. The re-design of a chosen compliant mechanism using the parameter curves.

Two governing equalities for an accelerometer arise from the static equilibrium equations (Eqs. (1)–(2)) with the input force and the output force taken as $m_a a$ and $m_{ext} a$, respectively. The third equality arises because of the natural frequency requirement, i.e., Eq. (4a). These three equations are the governing equations that we need to draw the stiffness and inertia maps.

In order to generate the stiffness map for user-specifications, the three governing equations can be simultaneously solved for the three SL parameters k_{ci}, k_{co} and n in terms of m_{ci}, m_{co}, and the rest of the specification variables listed above. Thus, we get

$$\begin{aligned} k_{ci} &= k_{ci}(\{m_{ci}, m_{co}\}, \text{specification variables}) \\ k_{co} &= k_{co}(\{m_{ci}, m_{co}\}, \text{specification variables}) \\ n &= n(\{m_{ci}, m_{co}\}, \text{specification variables}) \end{aligned} \tag{16}$$

As the specification variables have minimum and maximum values, there exists a large set of values for $\{k_{ci}, k_{co}, n\}$ for a given cursor position $\{m_{ci}, m_{co}\}$ in the $m_{ci} - m_{co}$ plot. For simplicity and to draw a bounded region on a $k_{ci} - k_{co}$ graph, only two of the variables on the right-hand-side of Eq. (16) are allowed to have bounds. One of the them is chosen to be the input displacement, u_{in}, and the other is the natural frequency, ω_1.

Two case studies are discussed here to illustrate the design methodology.

4.2.1. Problem 1

The following specifications are used: $a_{\min} = 9.81$ kg/ms^2, $m_a = 1.5\times10^{-7}$ kg, $k_a = 2000$ N/m, $m_{ext} = 7\times10^{-9}$ kg, $k_{ext} = 1$ N/m, $u_{out} = 5.6\times10^{-9}$ m and $\omega_1 = 8$ kHz–8.5 kHz. This is equivalent to a net performance enhancement of around eight times when compared with a case of not using a DaCM. The upper and lower bound for the values of u_{in} are chosen dynamically depending on the cursor location in the inertia plot such that it yields positive values for k_{ci} and k_{co}. Note that the aforementioned values for the inertia and stiffness of the suspension depend on the chip-area available to the designer and the constraints of the chosen manufacturing process.

In order to choose a compliant mechanism for redesign, each mechanism in the database is chosen and its stiffness map is generated for the $\{m_{ci}, m_{co}\}$ values of that mechanism. In other words, the cursor location in the inertia plot is moved from one mechanism to the other. As this is done for each mechanism, the distance of its $\{k_{ci}, k_{co}\}$ and the feasible map is measured and the mechanisms are numbered according to the closeness of the aforementioned distance. The mechanism whose $\{k_{ci}, k_{co}\}$ is the closest to its feasible stiffness map is chosen for modification. In this case, such a mechanism happens to be the mechanism shown in Fig. 13(a) and the corresponding stiffness map is shown in Fig. 13(b).

The parameter curves are then drawn from the current point. Although, a maximum of five curves corresponding to the design parameters listed in Fig. 10 can be drawn from the current point, for the sake of clarity, only the curve that gives incremental change in width is shown in Fig. 14. As we move along this curve in the $k_{ci} - k_{co}$ plot, the cursor location in the inertia plot is

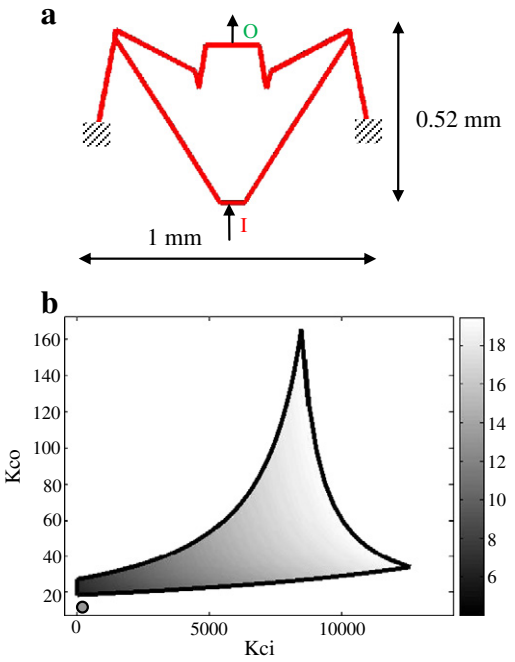

Fig. 13. a) The selected mechanism with its dimensions and b) the initial feasible map obtained for the selected mechanism ($m_{ci} = 1.6\times10^{-8}$ kg, $m_{co} = 9.64\times10^{-10}$ kg, minimum in-plane width of 2.4 μm).

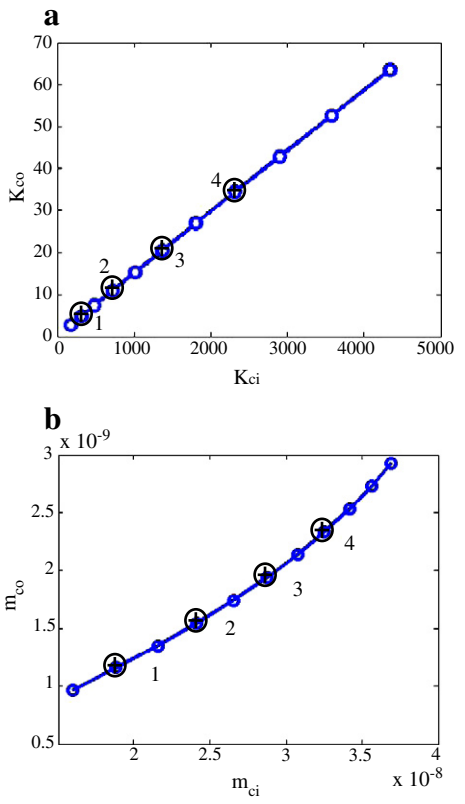

Fig. 14. The minimum width curve on a) the stiffness plot and b) the inertia plot, corresponds to incremental changes in widths of the mechanism. Dots 1, 2, 3 and 4 correspond to minimum in-plane widths of 2.4 μm, 3.2 μm, 4.0 μm and 5.2 μm respectively.

moved along the changing $\{m_{ci}, m_{co}\}$ of the mechanism. Since the $\{m_{ci}, m_{co}\}$ of the modified mechanism is used to generate the feasible stiffness map, its location and shape change at every design modification step as shown in Fig. 15(a)–(c). The dependence of the stiffness map on the m_{ci} and m_{co} of the mechanism is shown by successive feasible maps that are shown for incremental changes in widths of all the beam elements of the mechanism. In Fig. 15, the feasible map corresponding to the current state is shown by a solid line while the stiffness maps corresponding to the previous states of the mechanism are shown by dashed lines. As shown in Fig. 16, along the parameter curve, there is a matching of underlying n of the point in the feasible map and n of the mechanism. This indicates that the current modified mechanism satisfies the user specifications.

4.2.2. Problem 2

Consider a design problem where the mechanism topology is already selected by the user, as shown in Fig. 17(a). This is an inverting-type mechanism which is chosen due to some favorable factors such as anchor positions, layout and location and orientation of the input and the output points of the mechanism. The current minimum feature size is 10 μm and the overall

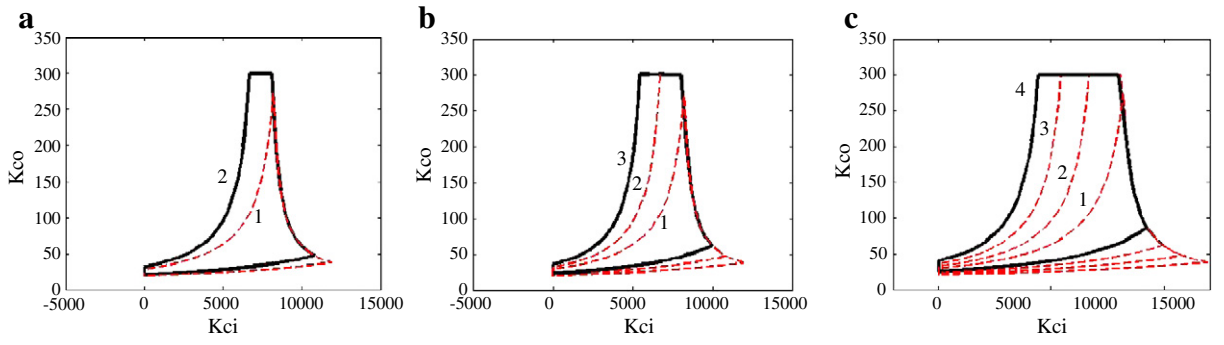

Fig. 15. The dependence of the stiffness maps on $m_{ci}$and m_{co} of the mechanism.

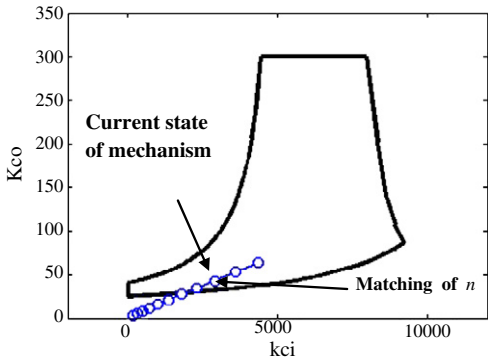

Fig. 16. There is a matching of n inside the feasible map indicating that the current state of the mechanism (width of 5.2 μm) satisfies the specifications.

size in X and Y-directions is 2.8 mm and 0.8 mm respectively. The chosen manufacturing process is MUMPS- multi-user MEMS processes, where the minimum feature size that can be reliably manufactured is 6 μm. The designer has a constraint that the overall size in both the orthogonal directions should not exceed 4 mm.

The other user-specifications are: $a_{\min} = 9.81\ \text{m/s}^2$, $m_a = 6.0\times10^{-7}$ kg, $k_a = 20$ N/m, $m_{ext} = 1\times10^{-8}$ kg, $k_{ext} = 0.08$ N/m, $u_{out} = 6\times10^{-7}$ m and $\omega_1 = 5$ kHz–6 kHz. This is equivalent to a net performance enhancement of around 2 times when compared with a case of not using a DaCM. As noted earlier, the upper and lower bound for the values of u_{in} are chosen dynamically to give positive values for k_{ci} and k_{co}; the user need not specify them. It is found that, there are no values for u_{in} that can give positive values for k_{ci} and k_{co}; the feasible stiffness map is null. This implies that the user-specifications cannot be met by the mechanism. Knowing this a-priori is one of the important features of our method.

However, if the frequency constraint is relaxed to only 0.9 kHz–1.1 kHz, then the feasible stiffness map is not null and is as shown in Fig. 17(b). Although the feasible map extends much above, it is shown only up to a value of $k_{co} = 70$. The reason for the existence of the extended feasible map becomes clear from Fig. 17(c) and (d), where k_{ci} and k_{co} go to infinity for some values of u_{out}/u_{in}. Note that the shape of the stiffness map is markedly different from that in Fig. 15 because in this case the mechanism

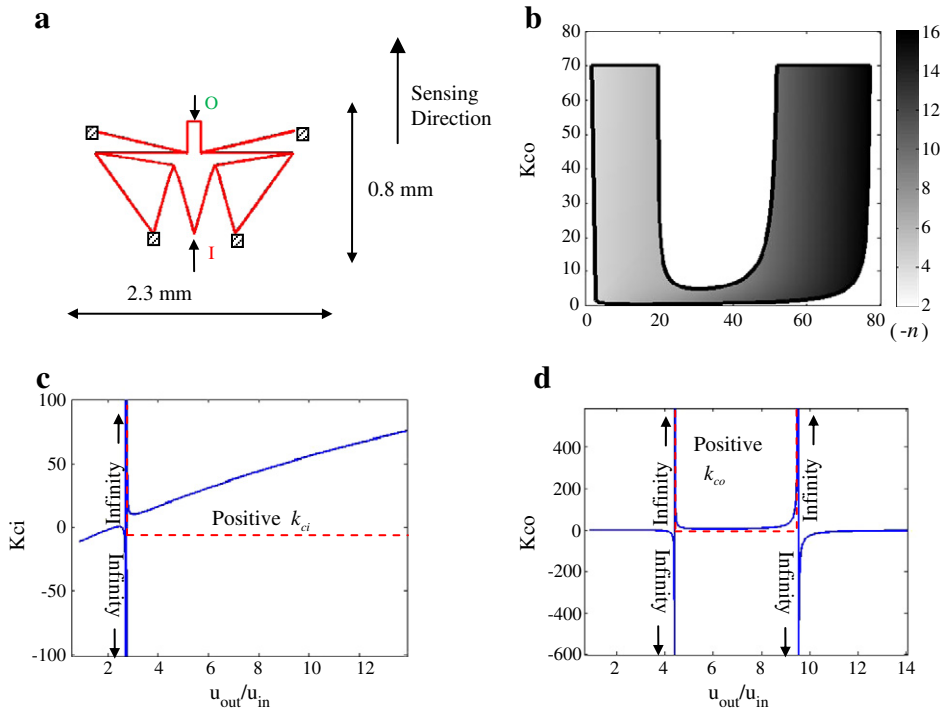

Fig. 17. a) The selected mechanism with its dimensions and b-d) the initial feasible map and related plots obtained for the selected mechanism ($m_{ci} = 2.98\times10^{-8}$ kg, $m_{co} = 1.55\times10^{-9}$ kg, minimum in-plane width of 10 μm).

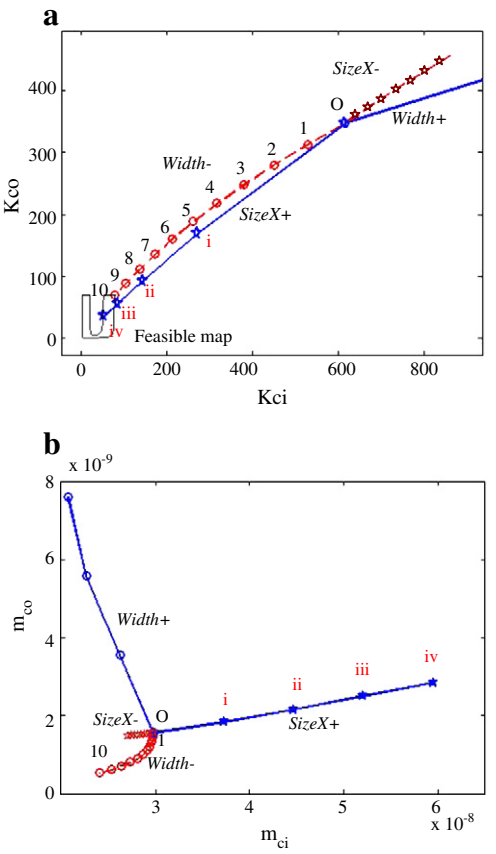

Fig. 18. The minimum width curve and the size in X-direction curves on a) the stiffness plot and b) the inertia plot.

chosen is an inverter where the direction of the displacement at the output is different from the applied inertia force. The gray scale bar in Fig. 17(b) shows the value of $(-n)$. The next step is to re-design this mechanism so that the user-specifications are met, which is explained next.

Four curves emanating from (k_{ci},k_{co}) and (m_{ci},m_{co}) of the original mechanism, marked as O, are shown in Fig. 18(a)–(b). The solid curves with markers, star $(*)$ and circle $(\circ)$, indicate the parameter curves obtained when the in-plane width and the size in *X*-direction are increased from their current values. These are marked as *Width* + and *SizeX* + in the Fig. 18(a–b). The dashed curves with markers, star $(*)$ and circle $(\circ)$, indicate the parameter curves obtained when the in-plane width and the size in *X*-direction are reduced from their current values. These are marked as *Width*- and *SizeX*- in the Fig. 18(a–b).

From Fig. 18(a), it is clear that *Width*- curve and the *SizeX* + curve lead towards the feasible stiffness map. If the *SizeX* + curve is chosen, it lands inside. But the overall size in the X-direction (represented by dot *iv* in Fig. 18(a)) is 4.63 mm, which is not acceptable to the designer. The designer, instead of selecting the *SizeX* + first, selects the *Width*- curve as the first step of re-design. This curve is followed until dot 8 in the Fig. 18(a) where the minimum feature size becomes 6 um. This is the minimum feature size allowable with the chosen manufacturing process. Note that the feasible stiffness map changes as we move along the curve, but the changes are very small. These small changes are shown in Fig. 19(b).

From the dot 8 in Fig. 18(a), we draw the *sizeX* + curve as shown in Fig. 19(a). As we move along this curve, (the very first dot, *i*, in Fig. 19(a)), we find that there is a matching of *n* of the compliant mechanism and the underlying *n* inside the map. The overall size in the X-direction corresponding to this dot *i* is 3.09 mm, indicating the space constraint is also adhered to. The movement of the cursor in the inertia plot is shown in Fig. 19(c).

4.3. Design of a compliant valve

In this section, we explain how the SML model can be used in the design of a valve where the requirement is that the input and the output ports have to move by specified distances in a specified time. The framework adopted here is similar to the one adopted in the previous case of accelerometer.

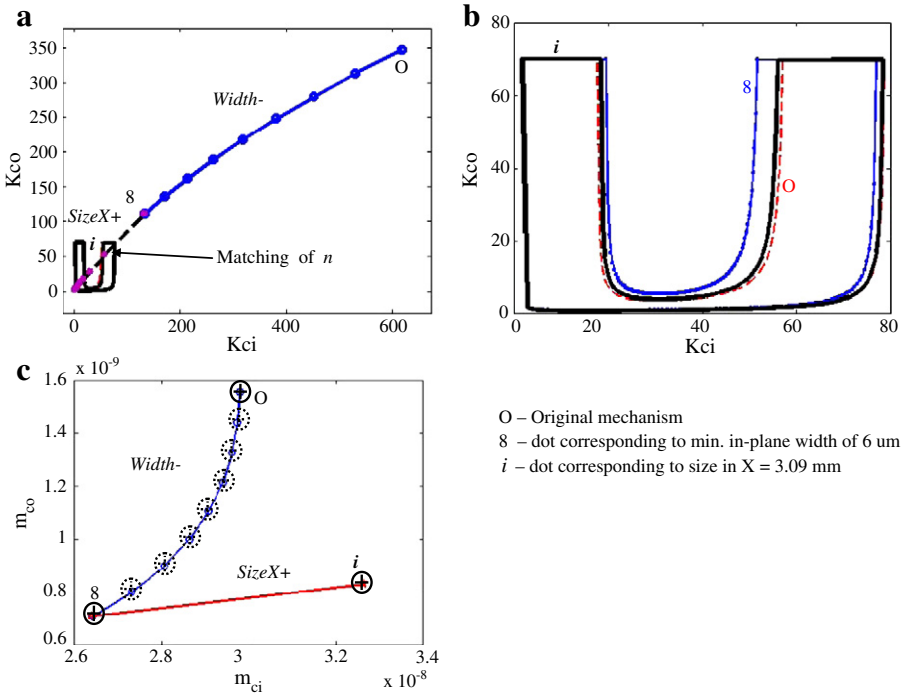

Fig. 19. There is a matching of n inside the feasible map indicating that the current state of the mechanism (width of 6 μm and size in X-direction = 3.09 mm) satisfies the specifications.

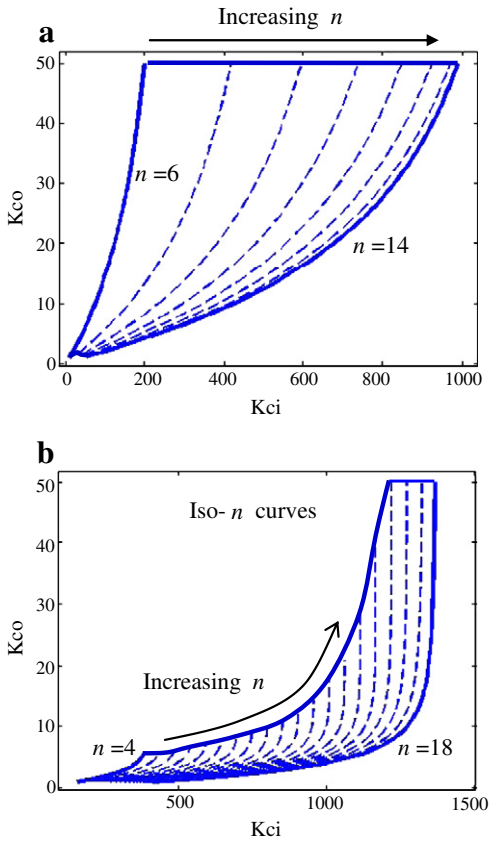

Fig. 20. The iso-n curves shown in (a) help in creating the feasible map (b) with a different set of specifications.

The force generated by the actuator is assumed to be in the form of a step excitation of magnitude F_{in}. The output port has to move against a steady external load F_{out}. The performance requirement is that the input and the output ports have to move by distances u_{in} and u_{out} respectively in a specified time t. The following specifications are used in this illustrative example: $F_{in} = 1$ N, $m_a = k_a = k_{ext} = m_{ext} = 0$, $F_{out} = 0.02$ N, $u_{in} = 0.001$ m and $u_{out} = 0.01$ m. The prescribed time is taken as 0.03 s. Note that the specification of prescribed time is chosen such that the re-design stage can be explained in simple steps. The governing equation that is of concern here is Eq. (13), which is in terms of the SML parameters and the aforementioned specification variables. This enables us to draw a feasible map as explained next.

In order to draw the feasible stiffness map, a number of iso-n curves are generated on the $k_{ci} - k_{co}$ graph, which indicates the (k_{ci},k_{co}) pairs along this iso-n curve that satisfy the governing Eq. (13). Note that $\{m_{ci}, m_{co}\}$ used to generate these corresponds to the cursor location in the inertia plot. These iso-n curves make up for a region called as the feasible stiffness map for this problem, as shown in Fig. 20(a). When the cursor location in the inertia plot corresponds to the mechanisms' m_{ci} and m_{co}, every point (k_{ci},k_{co}) inside the feasible map as shown in Fig. 20(a) along with an appropriate n satisfies the user requirements. Fig. 20(a) shows the iso-n curves generated for the compliant mechanism in Fig. 8, and for the aforementioned specification variables. Fig. 20(b) is generated for a different set of specifications ($F_{in} = 1$ N, $m_a = k_a = k_{ext} = m_{ext} = F_{out} = 0$, $u_{in} = 0.003$ m and $u_{out} = 0.024$ m) to illustrate the difference in the shapes of the feasible stiffness maps in accordance with the user-specifications.

In order to choose the compliant mechanism for re-design, the stiffness map for each mechanism is generated and its distance from the mechanism's (k_{ci},k_{co}) is computed. Based on the closeness of the mechanism's (k_{ci},k_{co}) with its stiffness map, the mechanisms are numbered and the closest mechanism is chosen for re-design. Such a mechanism (shown in Fig. 8) has the following SML parameters: $k_{ci} = 1054.11$ N/m, $k_{co} = 24.73$ N/m, $n = 7.45$, $m_{ci} = 0.074$ kg, $m_{co} = 0.0031$ kg.

Fig. 21 illustrates the re-design stage. As shown in Fig. 21(a), the (k_{ci},k_{co}) of the initial mechanism lies outside the feasible map and is shown as dot 1. The cursor location in the inertia plot corresponds to the $\{m_{ci}, m_{co}\}$ of the current state of the mechanism, shown as dot 1 in Fig. 21(b). As we move across the decreasing width curve, the feasible stiffness map changes as shown in Fig. 21(a). Dot 2 is still not inside the feasible map. As the width is further decreased, dot 3 corresponding to the current mechanism lies inside the feasible map, as shown in Fig. 21(a), with a matching n indicating the current mechanism satisfies the user specifications. The successive cursor locations, 1, 2 and 3, in the inertia plots are shown in Fig. 21(b).

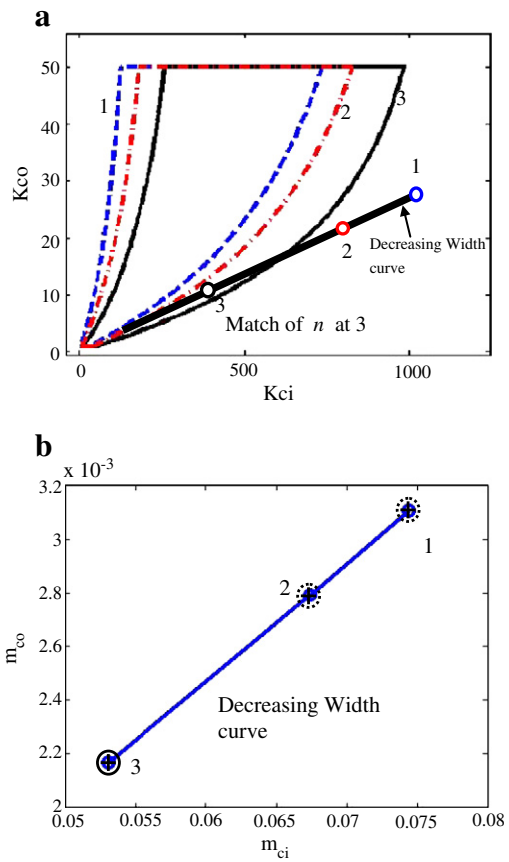

Fig. 21. The feasible map in the case of the transient compliant valve: the map changes as the mechanism is modified. Dots 1, 2 and 3 correspond to mechanisms corresponding to minimum width of 1 mm, 0.9 mm and 0.7 mm respectively.

5. Closure

A spring-mass-lever model is introduced in this paper. It has five parameters, two lumped masses at the input and output ports, two spring stiffnesses at input and output and a lever ratio. The use of SML model in quick dynamic analysis of a large system is demonstrated in this paper. The frequency estimates obtained in this paper using the SML model are close within 2% error to the estimates obtained with the complete FE model. Furthermore, the transient response under transient analysis predicted by the SML model is compared with the complete FE model and is also found to be close within 18% error. The use of SML model in the design of a capacitive accelerometer is explained by introducing the concepts of stiffness and inertia maps. The use of SML model in the design of a compliant valve with specified transient behavior is also demonstrated.

Appendix A

The data pertaining to the accelerometer analysis example of Section 3.1 is included in this appendix. The values of k_{ci}, k_{co}, and n for the DaCMs M_1 used in this example were obtained as: 1636.7 N/m, 5.63 N/m and 50.08 respectively. The values of k_{ci}, k_{co}, and n for the DaCMs M_2 were obtained as: 636.94 N/m, 359.92 N/m and −5.97 respectively. Tables A1–A3 indicate the data related to the other parameters needed for the SML model.

Table A1: Input side calculations.
Table A2: Output side calculations.
Table A3: Calculation of m_{ci} and m_{co}.

Device	Eigenfrequency (Hz)	Stiffness k_a (N/m)	Effective mass m_a (kg)
S_1	918.10	77.53	2.33×10^{-6}
S_2	35159	3806.33	7.80×10^{-8}

Device	Eigenfrequency (Hz)	Stiffness k_{ext} (N/m)	Effective mass m_{ext} (kg)
S_1	331.24	0.58	1.34×10^{-7}
S_2	10990.84	17.67	3.70×10^{-9}

Mechanism	TKE (1st loading case)	TKE (2nd loading case)	m_{ci} (kg)	m_{co} (kg)
M_1	4.09×10^{-13}	1.27×10^{-9}	7.84×10^{-8}	8.43×10^{-10}
M_2	1.57×10^{-14}	5.98×10^{-13}	4.22×10^{-9}	2.40×10^{-10}

Appendix B

The following equations defined the expressions for the symbols used in Eqs. (10–12) cited in Section 3.2.

$$K_{11}=\frac{k_3b+c\sqrt{b}}{2m_{co}^2k_2^2}$$

$$K_{11}=\frac{k_3b-c\sqrt{b}}{2m_{co}^2k_2^2}$$

$$m_{11}=b+\frac{(k_1m_{co}-m_{ci}k_3)\sqrt{b}}{m_{co}k_2^2}$$

$$m_{22}=b+\frac{(-k_1m_{co}-m_{ci}k_3)\sqrt{b}}{m_{co}k_2^2}$$

$$\begin{cases} a=m_{ci}k_3+k_1m_{co} \\ b=m_{ci}^2k_3^2-2m_{ci}k_3k_1m_{co}+k_1^2m_{co}^2+4m_{ci}m_{co}k_2^2 \\ c=k_1k_3m_{co}-m_{ci}k_3^2-2m_{co}k_2^2 \end{cases} \qquad \begin{cases} k_1=k_{ci}+k_a+n^2k_{co} \\ k_2=-nk_{co} \\ k_3=k_{co}+k_{ext} \end{cases}$$

$$\phi_{11}=\frac{m_{ci}k_3-k_1m_{co}+\sqrt{b}}{2\sqrt{b}}$$

$$\phi_{12}=-\frac{m_{co}k_2}{\sqrt{b}}f_1=F_1+\left(\frac{\frac{a-\sqrt{b}}{2m_{co}}-k_1}{k_2}\right)F_2f_2=F_1+\left(\frac{\frac{a-\sqrt{b}}{2m_{co}}-k_1}{k_2}\right)F_2$$

References

[1] L.L. Howell, Compliant Mechanisms, John-Wiley, New York, 2001.
[2] L.L. Howell, A. Midha, Parametric deflection approximations for end-loaded, large-deflection beams in compliant mechanisms, Journal of Mechanical Design, Transactions of the ASME 117 (March 1995) 156–165.

[3] L.L. Howell, A. Midha, A loop-closure theory for the analysis and synthesis of compliant mechanisms, Journal of Mechanical Design, Transactions of the ASME 118 (March 1996) 121–125.
[4] N.O. Rasmussen, J.W. Wittwer, R.H. Todd, L.L. Howell, S.P. Magleby, A 3D Pseudo-Rigid-Body Model for Large Spatial Deflections of Rectangular Cantilever Beams, *Proceedings of IDETC/CIE 2006* as part of the 2006 ASME Mechanisms & Robotics Conference, Philadelphia, PA, DETC2006-99465, 2006.
[5] C.P. Lusk, L.L. Howell, Components, building blocks, and demonstrations of spherical mechanisms in microelectromechanical systems, Journal of Mechanical Design 130 (March 2008).
[6] M. Frecker, G.K. Ananthasuresh, S. Nishiwaki, N. Kikuchi, S. Kota, Topological synthesis of compliant mechanisms using multi-criteria optimization, Journal of Mechanical Design, Transactions of the ASME 119 (2) (June 1997) 238–245.
[7] S.R. Deepak, M. Dinesh, D. Sahu, G.K. Ananthasuresh, A comparative study of the formulations and benchmark problems for the topology optimization of compliant mechanisms, ASME Journal of Mechanisms and Robotics 1 (1) (2008) 20–27.
[8] M.P. Bendsøe, O. Sigmund, Topology Optimization: Theory, Practice, and Applications, Springer, New Cork, 2003.
[9] G.K. Ananthasuresh (Ed.), Optimal Synthesis Methods for MEMS, Kluwer, Ámsterdam, 2003.
[10] L. Yin, G.K. Ananthasuresh, J. Eder, Optimal design of a cam-flexure clamp, Finite Elements in Analysis and Design 40 (2004) 1157–1173.
[11] G. Krishnan, G.K. Ananthasuresh, A systematic method for the objective evaluation and selection of compliant displacement amplifying mechanisms for sensor applications, Journal of Mechanical Design 130 (10) (2008) 102304:1–102304:9.
[12] G. Krishnan, C. Kim, S. Kota, Compliant mechanism design using a building block approach, ASME International Design Engineering Technical Conferences, Montreal, Canada, August 2010.
[13] S. Hegde, G.K. Ananthasuresh, Design of single-input–single-output compliant mechanisms for practical applications using selection maps, Journal of Mechanical Design 132 (August 2010) 081007-1–081007-8.
[14] M.Y. Wang, A kinetoelastic formulation of compliant mechanism optimization, Journal of Mechanisms and Robotics 1 (May 2009) 021011-1–021011-10.

Sudarshan Hegde received his B.E. in Mechanical Engineering from Walchand College of Engineering, Sangli, Maharashtra, India in 2003. He worked at Bharat Forge Ltd. Pune, India for a year before joining M.E (Mechanical Engg.) at Indian Institute of Science, Bangalore, India. He is currently a doctoral student (2006–present) at Indian Institute of Science, Bangalore. His research interests include compliant mechanisms, topology optimization and finite element methods.

G.K. Ananthasuresh (B. Tech. IIT-Madras, 1989; PhD, Michigan, 1994) is a Professor of Mechanical Engineering in the Indian Institute of Science, Bangalore, India. His previous positions include Associate Professor in University of Pennsylvania and visiting professorships in University of Cambridge, UK, and Katholike Univesiteit, Leuven, Belgium. His current research interests include compliant mechanisms, kinematics, multi-disciplinary design optimization, microsystems technology, micro and meso-scale manufacturing, protein design, and cellular biomechanics. He serves on the editorial boards of six journals and is a co-author of more than 160 papers in journals and conferences as well as one edited book and nine book-chapters. He is a recipient of the NSF Career Award in the USA and the Swarnajayanthi Fellowship in India as well as five best paper awards in international and national conferences.